Ag-TiO_2/EVA Composites for Wood Preservation: Antibacterial, Anti-mold, and Anti-Discoloration Performance

Ting Liu, Yaoxing Sun,* Honggang Zhao,* Huachun Qi, and Jiuyin Pang

Ag-TiO_2/EVA composites were synthesized using silver-loaded nano TiO_2 (Ag-TiO_2) and ethylene-vinyl acetate (EVA) emulsion as raw materials, aiming to develop functional materials with antibacterial, anti-mold, and anti-discoloration in properties for wood protection. The study systematically evaluated the composites' inhibition efficacy against discoloration fungi and molds, long-term antibacterial performance, as well as the tensile strength and water vapor transmission rate of composite films. Experimental results demonstrated that 100% inhibition efficacy against *Botryodiplodia theobromae* and *Aspergillus niger* was achieved under two optimal conditions: film thickness of 0.12 to 0.15 mm with Ag-TiO_2 loading ≥20%, or film thickness of 0.18 to 0.21 mm with Ag-TiO_2 loading ≥15%. Samples with 10%, 15%, and 20% Ag-TiO_2 loading exhibited >99.99% antibacterial rates against both *Escherichia coli* and *Staphylococcus aureus*. Notably, the 20% Ag-TiO_2 sample retained high antibacterial values of 93.0% and 91.7% against these bacteria after 15 days of storage. Mechanical and barrier property tests revealed that compared to the control, the tensile strength of composite films increased by 19.8%, 24.6%, and 29.3% at Ag-TiO_2 loadings of 10%, 15%, and 20% respectively, while water vapor transmission rates decreased by 48.6%, 52.9%, and 60.6%. These findings collectively confirm that Ag-TiO_2/EVA composites possess excellent bactericidal effects and significant wood anti-mold/anti-discoloration functionality.

DOI: 10.15376/biores.20.3.7194-7210

Keywords: Composite material; Wood mold resistance; Antibacterial; EVA

Contact information: Key Laboratory of Wooden Materials Science and Engineering of Jilin Province, School of Material Science and Engineering, Beihua University, Jilin 132013, China;
** Corresponding author: sunyaoxing@sina.com (Y.S); mailzhaoyang@163.com (H.Z)*

INTRODUCTION

Wood, as a renewable natural biomaterial, is widely utilized in construction, furniture, and decorative applications (He *et al.* 2021; Jian *et al.* 2022; Chen *et al.* 2022). However, its susceptibility to microbial degradation leads to decay, mold growth, and discoloration, significantly compromising its functional value and aesthetics (Zhang *et al*. 2016; Selim *et al*. 2017; Teng *et al*. 2018; Emmerich *et al*. 2021). To address these issues, researchers have dedicated efforts to developing effective wood preservation technologies. Surface treatments, such as applying chemical preservatives, are common industrial practices. Preservatives such as chromated copper arsenate (CCA), pentachlorophenol, and copper naphthenate are widely used for their antimicrobial properties. However, these chemicals contain toxic components such as arsenic and chromium, posing risks to human

health and the environment (Cao 2006; Yang 2011; Xi and Jiang 2013; Sun *et al.* 2017; Yang *et al.* 2021; Donald *et al.* 2022).

Traditional organic compounds as preservatives have certain drawbacks, leading researchers to focus on the efficacy of inorganic metals as wood preservatives. The use of inorganic metals and metal oxides as antimicrobial agents is already widespread, with metals such as Ag, Au, and TiO_2 being the most common and extensively applied metal-based antimicrobial materials (Zhang and Chen 2009; Zhao *et al.* 2012; Shams *et al.* 2019). Many researchers have utilized inorganic metals as effective bactericidal components in antibacterial agents, where metal ion release disrupts cellular structures and inhibits bacterial growth (Cui *et al.* 2012; Lipovsky *et al.* 2013; Jin *et al.* 2014; Su *et al.* 2019; Li *et al*. 2020; Persaud *et al.* 2020). Notably, Ag and TiO_2 are particularly favored. Gunputh *et al.* (2020) and Mohandas *et al.* (2017) combined Ag and TiO_2 by layering Ag on TiO_2 surfaces, thereby achieving effective bactericidal effects against *E*. *coli* and *S*. *aureus*. The Ag-TiO_2 nanoparticles used in this composite integrate the antibacterial properties of both Ag and TiO_2: TiO_2 exhibits strong bactericidal effects under light irradiation, while Ag retains antibacterial activity even in dark conditions, enabling 24-h protection (Sreeja and Shetty 2017). However, inorganic metal antibacterial agents alone cannot meet long-term requirements, and conventional wood preservatives also fail to ensure sustained efficacy.

In order to achieve long-lasting antibacterial effects, delay the release of Ag-TiO2, and enhance the antibacterial efficacy, this study prepared Ag-TiO2/EVA composite materials by mixing Ag-TiO_2 with ethylene-vinyl acetate copolymer (EVA). EVA, a common polymer with excellent film-forming and mechanical properties, serves as an ideal carrier for Ag-TiO_2. Borreguero *et al.* (2011) prepared phase-change microcapsules encapsulating wax with low-density polyethylene (LDPE)/EVA *via* spray drying. The microencapsulation efficiency reached 63%, and the resulting microcapsules exhibited not only excellent mechanical properties but also enhanced phase-change cycling stability (up to 3,000 cycles), demonstrating heat storage capacity comparable to industrialized polystyrene-based phase-change microcapsules. Ag-TiO_2/EVA not only combines the antibacterial properties of Ag-TiO_2 and the excellent physical properties of EVA, but also protects Ag-TiO_2 through the protective effect of EVA, preventing its rapid loss, thereby achieving long-lasting antibacterial and mold-preventing effects.

This study developed a wood protective material with antibacterial, anti-mold, and anti-discoloration functions, namely Ag-TiO_2/EVA micro-composite, which was applied to wood surfaces to form an antibacterial film. The objective was to enhance wood resistance against bacteria, mold, and discoloration, thereby protecting wood from fungal and mold infestations. Through the preparation of Ag-TiO_2/EVA micro-composites, the research investigated their application potential in wood preservation, aiming to meet industry requirements for novel non-toxic, harmless, and long-lasting anti-mold agents with sustained efficacy.

EXPERIMENTAL

Materials

Populus ussuriensis Kon. specimens were collected from the Sanhe Forest Farm, Jiaohe Forestry Experimental Zone Administration, Jilin Province, China, for laboratory experiments on mold resistance and discoloration prevention. A sapwood board of *P. ussuriensis* with straight grain, no decay or discoloration, and uniform texture was selected

(density: 0.440g/cm^3 kg/m^3; moisture content: 12%). The longitudinal direction of the wood was aligned with the length axis. The board was processed into three types of test specimens: Mold resistance testing: 192 specimens of dimensions 50 mm (L) × 20 mm (W) × 5 mm (T). Antimicrobial testing: 96 specimens of dimensions 50 mm (L) × 50 mm (W) × 5 mm (T). Film adhesion testing: 90 rectangular specimens of dimensions 150 mm (L) × 100 mm (W) × 10 mm (T). All samples were dried by an electric heating constant temperature blast drying oven (DHG-9075A, Shanghai Yiheng Technology Corporation) at 103° before use.

The ethylene-vinyl acetate (EVA; industrial grade) emulsion (Dalian Chemical (Jiangsu)) had a solids content of 55% and a viscosity of 4800 mPa·s. Other materials used included silver-loaded nano TiO_2 (VK-T06, 1% Ag content, industrial grade, Hangzhou Tuoming New Materials), Sodium chloride (NaCl; analytical grade), agar powder, yeast extract, glucose, beef extract, and peptone (Beijing Aoboxing Biotechnology).

Escherichia coli and *Staphylococcus aureus* were provided by Jilin Provincial Engineering Research Center of Forestry Biotechnology. The molds *Aspergillus niger* and *Botryodiplodia theobromae* Pat. were provided by the China Center for Forest Microbial Culture Collection.

Preparation of Ag-TiO_2/EVA Composite Materials

The Ag-TiO_2/EVA composite emulsion was synthesized *via* high-temperature melt bonding technology by leveraging the adhesion of EVA emulsion to construct a stable structure of EVA and Ag-TiO_2. EVA was placed in a beaker and heated to a viscous fluid state at 130 °C in an oil bath. Ag-TiO_2 was then gradually added at mass ratios of Ag-TiO_2 to EVA of 1:9, 1.5:8.5, and 2:8. Utilizing the cohesive strength of EVA, Ag-TiO_2 was tightly integrated under continuous high-temperature stirring until a homogeneous mixture formed, ultimately yielding the Ag-TiO_2/EVA micro-composite material emulsion.

Preparation of Ag-TiO_2/EVA Antimicrobial Films

The prepared Ag-TiO_2/EVA micro-composite material emulsion was mixed and then poured into a polytetrafluoroethylene (PTFE) mold at the appropriate ratio, spread evenly on a water platform, and left at room temperature for 12 h to form films. The resulting films had four thicknesses: 0.12 to 0.15 mm, 0.15 to 0.18 mm, 0.18 to 0.21 mm, and 0.21 to 0.24 mm. After film formation, the samples were removed and equilibrated under 75% relative humidity for 72 h to balance moisture content.

Scanning Electron Microscopy (SEM) Characterization

The test samples were dried thoroughly at 120 °C for 4 h, then adhered to a specimen holder using conductive adhesive. After surface sputtering with gold, high-resolution scanning electron microscopy (SEM) was performed using an environmental scanning electron microscope (XL30-ESEM, Philips Instruments).

Fourier Transform Infrared Spectroscopy (FTIR) Analysis

The dried samples were analyzed using a Fourier transform infrared spectrometer (IRAffinity-1s, Shimadzu Corporation) at room temperature. A 2 g sample was dried in an electric thermostatic blower dryer at 120 °C for 4 h, followed by FTIR measurement in the range of 400 to 4000 cm^{-1} with a resolution of 2 cm^{-1} and 64 accumulations.

Tensile Strength Testing of Antimicrobial Films

Following the GB/T 1040.3 (2006) standard, Ag-TiO_2/EVA films with four thicknesses were equilibrated at 75% relative humidity for 72 h and then subjected to tensile strength testing on a universal mechanical testing machine (MWW-10, Jinan Tianchen Testing Machine Manufacturing). The tensile strength (σ_t) was calculated using Eq. 1,

$$\sigma_t = \frac{P}{bd} \quad (1)$$

where σ_t is tensile strength of the film (MPa), P is maximum load (N), b is film width (mm), and d is film thickness (mm).

Water Vapor Permeability Testing

Water vapor transmission rate (WVTR) was measured according to GB/T 1037-(2021). The prepared films were sealed over desiccant-filled weighing bottles using sealing wax, then weighed on an analytical balance with 0.001 g precision. The samples were placed in a desiccator containing a saturated sodium chloride solution and weighed every 24 h for 7 consecutive days. Three parallel experiments were conducted for each group.

The water vapor transmission rate (WVT; g/(m²·24 h)) was calculated using Eq. 2,

$$WVT = \frac{24 \times (m_1 - m_2)}{A \times t} \quad (2)$$

where m_1 is total weight of the weighing bottle on the 7th day (g), m_2 is initial weight of the weighing bottle (g), A is effective area of the bottle opening (m²), and t is total time interval between measurements (h).

Film Adhesion Testing

The adhesion of the film was tested according to GB/T 9286-1998 Test Method for Adhesion of Paint Films. A hexagonal blade cutter was used to make cuts on the film at a 45° angle relative to the wood grain direction, ensuring that all cuts penetrated through to the substrate surface. The process was repeated perpendicularly (90°) to the original cuts to form a grid pattern. A soft-bristle brush was then swept diagonally across the grid in both backward and forward directions several times to remove loose fragments. The adhesion grade was determined by observing the damaged area under a 4× magnifying glass and calculating the grid damage rate. Each specimen was tested at three random locations until consistent adhesion grades were obtained across all replicates.

The coating grid damage (%) is calculated using Eq. 3,

$$W = \frac{m}{25} \times 100\% \quad (3)$$

where W is the grid damage percentage, m is the number of damaged grids, and 25 is the total number of grids. The adhesion grading criteria were as follows: Grade 0 (w=0%), Grade 1 (0%<w<5%), Grade 2 (5%≤w<15%), Grade 3 (15%≤w<35%), Grade 4 (35%≤w<65%), and Grade 5 (w≥65%).

Antibacterial Performance Testing of Ag-Tio_2/EVA Films

The antibacterial activity was evaluated according to GB/T 21866 (2008). Prepared samples were immersed in saturated deionized water for 24 h, 3 days, 7 days, and 15 days. The sample was coated on the wood sample to form a coating, and the bacteria that had

been cultured to a fixed concentration were added to the tested sample for culture to ensure that the bacteria solution was in uniform contact with the sample. After incubation in a constant temperature incubator, bacteria were eluted from the samples using a sterilization eluate. Finally, the quantified eluate was added to the Petri dish, again incubated in a constant temperature incubator, and the number of colonies was determined by viable colony counting. The antibacterial efficacy (E_{ab}) was calculated using Eq. 4,

$$E_{ab} = (A-B)/A \times 100 \quad (4)$$

where E_{ab} is expressed as %, with four significant figures), A is an average recovered bacterial count on blank control samples after 24 h (CFU/sample), and B is an average recovered bacterial count on antibacterial-coated samples after 24 h (CFU/sample).

Mold Resistance

Preparation of poplar mold-resistant specimens

The Ag-TiO_2/EVA micro-composite material emulsion was uniformly coated on all six surfaces of Daqingyang poplar specimens, fully encapsulating them. Four film thicknesses were prepared: 0.12 to 0.15 mm, 0.15 to 0.18 mm, 0.18 to 0.21 mm, and 0.21 to 0.24 mm. For each thickness and sample type, 12 specimens were prepared: 6 specimens inoculated with *Aspergillus niger* (black mold), 6 specimens inoculated with *Lasiodiplodia theobromae* (cocoa pod rot fungus). Control specimens (12 per thickness, 6 for each fungus) were also prepared. Each group underwent three independent replicate experiments, resulting in a total of 192 specimens.

Fungal inoculation and infection

After inoculation, both mold-resistant and control specimens were placed in a constant temperature and humidity chamber at 25 ± 2 °C and 75% relative humidity for fungal infection. Mold resistance was evaluated after 4 weeks.

Evaluation of mold resistance and discoloration prevention

Following GB/T 18261 (2013), the infected specimens were graded into 5 levels based on infection area and characteristics, with infection values serving as quantitative indicators (Table 1).

Table 1. Discoloration and Grading of Specimens after Bacterial Infection

Infection Value	Area of Infection of the Specimen
0	No visible hyphae or mold spots on the specimen surface
1	Infected area < 1/4 of the specimen surface
2	Infected area between 1/4–1/2 of the specimen surface
3	Infected area between 1/2–3/4 of the specimen surface
4	Infected area > 3/4 of the specimen surface

According to the infection value in Table 1, the control efficiency can be calculated, which can be used to evaluate the anti-mold and anti-discoloration ability of the antifungal agent. The higher prevention efficacy value indicated a stronger ability, as determined by Eq. 5,

$$E_p = (1-\frac{D_1}{D_0}) \times 100\% \quad (5)$$

where E_p is prevention efficacy (%), D_1 is infection value of antifungal-coated specimens, and D_0 is infection value of control specimens.

SEM analysis of anti-mold and anti-discoloration treated samples

After subjecting the wood specimens to anti-mold and anti-discoloration treatments, the samples were sectioned along the wood grain direction. Specimens measuring 2 cm × 2 cm were oven-dried at high temperature for 4 h. The dried specimens were mounted onto the sample stage using conductive adhesive, followed by surface sputter-coating with gold to enhance conductivity. High-resolution scanning electron microscopy (SEM) was subsequently employed to examine the internal microbial infestation and structural changes within the specimens.

RESULTS AND DISCUSSION

Characterization of Ag-TiO_2/EVA structure

Infrared spectroscopy analysis of Ag-TiO_2/EVA

Figure 1 shows the FTIR spectra of EVA, Ag-TiO_2, and Ag-TiO_2/EVA. As shown in Fig.1a, the absorbance peaks at 1740, 2900, 1240, and 1020 cm^{-1} correspond to the C=O stretching vibration, C-H stretching vibration, and C-O stretching vibrations in EVA, respectively. From Fig. 1b, the peak at 566 cm^{-1} is attributed to the Ti-O-Ti vibration, while the peaks at 3415 cm^{-1} and 1644 cm^{-1} correspond to the stretching and bending vibrations of -OH groups. In Fig. 1c, the spectrum of Ag-TiO_2/EVA retained the main characteristic peaks of EVA, indicating that the addition of Ag-TiO_2 did not disrupt the backbone structure of EVA. However, compared to pure EVA, the composite exhibited a Ti-O-Ti absorption peak at 566 cm^{-1}, which confirms that Ag-TiO_2 has been mixed in the EVA.

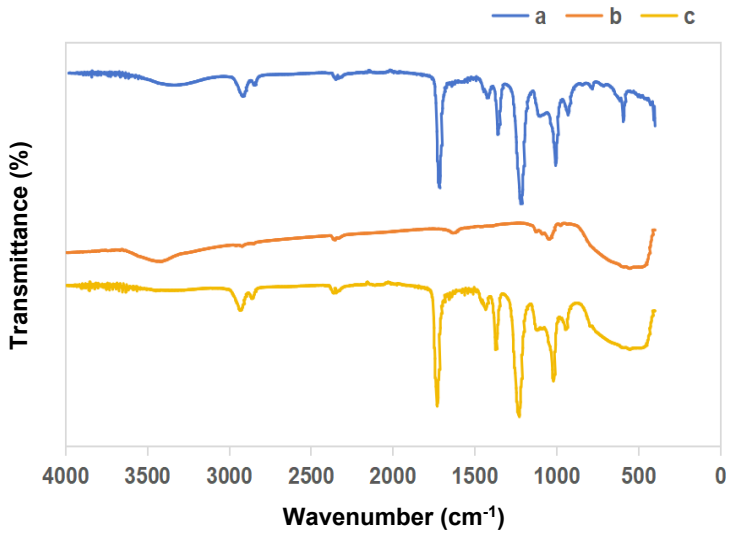

Fig. 1. FTIR spectrum of Ag-TiO_2/EVA (a) EVA; (b) Ag-TiO_2; (c) Ag-TiO_2/EVA

The absence of significant chemical bonding and the preservation of Ag-TiO_2's characteristic peaks in the composite suggest a predominantly physical combination, with the nanoparticle structure remaining intact. These results demonstrate that the incorporation of Ag-TiO_2 did not alter the chemical structure of EVA but primarily affected its physical properties, particularly those of the formed film.

Microscopic characterization of Ag-TiO2/EVA

Figure 2a displays the SEM image of the Ag-TiO2/EVA composite, where the composite particles exhibit a spherical morphology and aggregate together with an average particle size exceeding 1 um. Figure 2b, a magnified view of Fig. 2a, reveals distinct speckles on the surface of the Ag-TiO2/EVA particles, indicating the presence of Ag-TiO2 nanoparticles attached to the EVA shell. This observation demonstrates that high-intensity agitation during synthesis effectively mitigated agglomeration of Ag-TiO2, thereby facilitating its uniform distribution on the EVA surface.

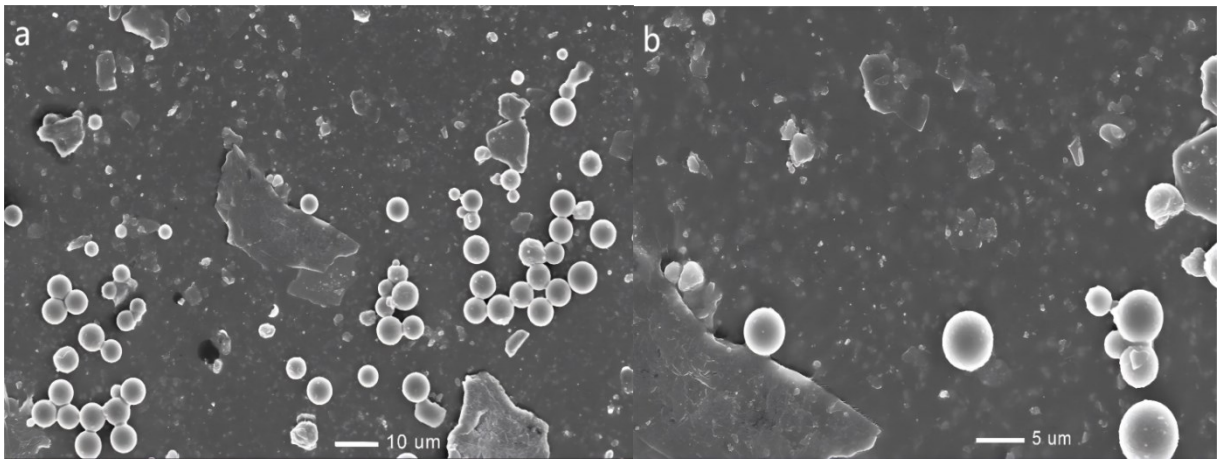

Fig. 2. SEM photographs of Ag-TiO2/EVA (a) Magnified 800 times; (b) Magnified 2000 times

Effect of Ag-TiO2 Loading on Properties of Antibacterial Films

Influence of Ag-TiO2 loading on tensile properties of films

As shown in Fig.3, the tensile strength of the antibacterial films progressively increased with higher Ag-TiO2 loading. When the Ag-TiO2 content was 0%, 10%, 15%, and 20%, the corresponding tensile strengths reached 6.12, 7.33, 7.63, and 7.92 MPa, respectively.

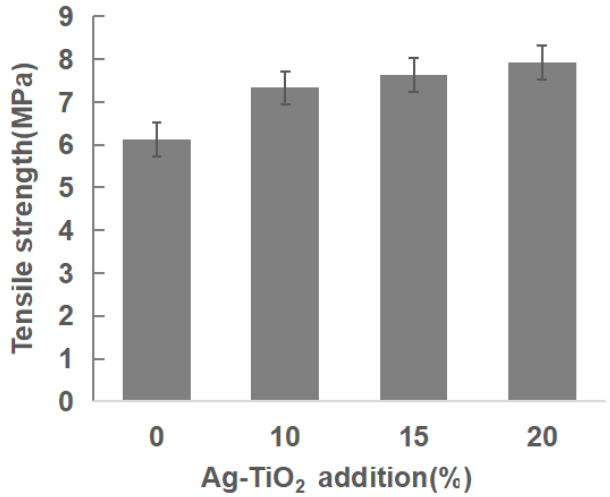

Fig. 3. Influence of Ag-TiO2 loading on tensile properties of films

Compared to the Ag-TiO_2-free film, these values represent tensile strength enhancements of 19.8%, 24.6%, and 29.3%, respectively. This enhancement can be attributed to two mechanisms: 1) Structural Stability: Increased Ag-TiO_2 content stabilizes the spherical morphology of Ag-TiO_2/EVA composites, where surface-bound Ag-TiO_2 nanoparticles enhance emulsion stability and elasticity. 2) Interfacial Reinforcement: Unencapsulated Ag-TiO_2 nanoparticles adsorbed at the oil-water interface via electrostatic interactions, forming uniformly dispersed nanocomposites. This effectively suppressed droplet coalescence and enhanced the mechanical integrity of the resultant films.

Collectively, the incorporation of Ag-TiO_2 demonstrated a dual-phase reinforcement effect, synergistically improving both emulsion stability and film tensile strength.

Influence of Ag-TiO_2 loading on water vapor transmission rate (WVTR) of films

As shown in Fig. 4, the water vapor transmission rate (WVTR) of the films decreased with increasing thickness under fixed conditions, primarily due to the extended diffusion pathways for water molecules in thicker films, which impeded their permeation. When the film thickness was maintained between 0.21 and 0.24 mm, the WVTR further decreased with higher Ag-TiO_2 loadings. At Ag-TiO_2 additions of 10%, 15%, and 20%, the WVTR reached minimum values of 10.64, 9.75, and 8.16 g/(m^2·24 h), respectively, representing reductions of 48.6%, 52.9%, and 60.6% compared to films without Ag-TiO_2.

The reduction in WVTR can be attributed to two factors. First, the Ag-TiO_2/EVA composite material particles have a smooth surface and are aggregated with each other, which physically obstructed the migration of water molecules. Second, the presence of Ag-TiO_2 nanoparticles reduced the available pathways for water diffusion within the film matrix. As the Ag-TiO_2 content increased, the density of these nanoparticles within the film increased, leading to a more pronounced restriction of water molecule movement and a corresponding decline in WVTR. This dual mechanism—combining geometric tortuosity from particle aggregation and nanofiller-induced barrier effects—effectively suppressed water vapor permeation. The results highlight the role of Ag-TiO_2 in simultaneously enhancing the barrier properties and structural integrity of the films, consistent with its previously demonstrated mechanical reinforcement effects.

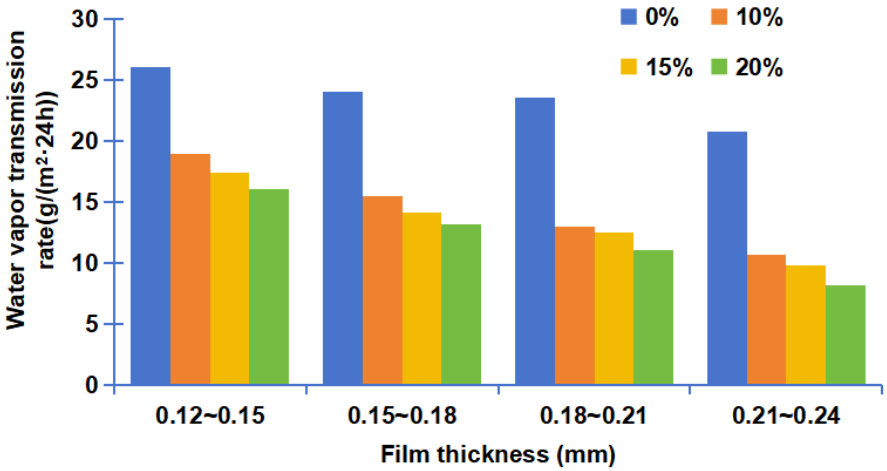

Fig. 4. Influence of Ag-TiO_2 loading on water vapor transmission rate of films

Influence of Ag-TiO2 loading on film adhesion testing

Adhesion refers to the bonding capacity between a coating and the substrate or between coating layers, serving as the prerequisite for the protective performance of the film. As shown in Fig. 5, the adhesion grade of the Ag-TiO2-incorporated film was identical to that of the pure EVA film, both achieving Grade 1. This indicates excellent post-film-formation adhesion, where the emulsion adheres firmly to the wood surface without delamination after application. The results demonstrate that the addition of Ag-TiO2 did not compromise the film's adhesion, and the modified emulsion retains the original superior physical properties of the EVA emulsion.

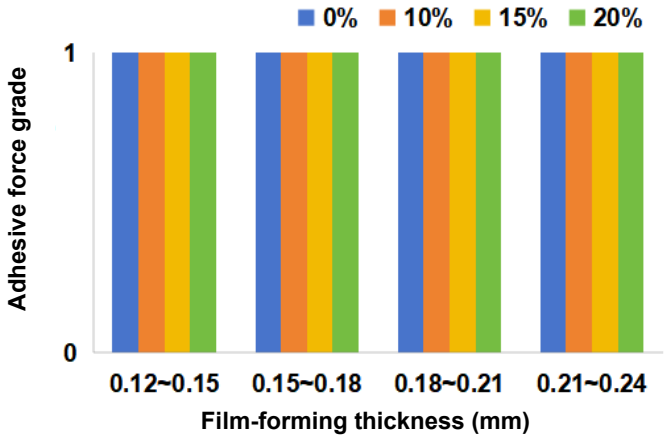

Fig. 5. Ag-TiO2/EVA Antibacterial film adhesion grade

Antibacterial performance of Ag-TiO2/EVA films

The antibacterial mechanism of Ag-TiO2/EVA composites is based on the release of metal ions (*e.g.*, Ag+) from Ag-TiO2 nanoparticles, which disrupt bacterial cell membranes. The protective effect of EVA ensures the slow and continuous release of Ag-TiO2, thereby providing a long-lasting sterilization effect. As shown in Figs. 6a and 6c, samples containing Ag-TiO2 soaked in saturated deionized water for 1 day (1D), 3 days (3D), 7 days (7D), and 15 days (15D) exhibited significant antibacterial effects after 24 h (24H) of incubation. Ag-TiO2-loaded samples showed no bacterial colony growth in the culture medium after 1D of soaking, only a single colony after 3D, sparse colonies after 7D, and minimal colony growth even after 15D. In contrast, the 0% Ag-TiO2 control samples were fully colonized by bacteria.

Quantitative results (Figs. 6b and 6d) demonstrated that all Ag-TiO2-containing samples achieved antibacterial efficacies exceeding 99.99% against both *E. coli* and *S. aureus* after 24 h of incubation. Over time, the sustained release of Ag-TiO2 from the composite maintained strong antibacterial performance. For the 20% Ag-TiO2 sample, antibacterial efficacies remained at 93.01% (*E. coli*) and 91.67% (*S. aureus*) even after 15D. The 10% Ag-TiO2 sample, though slightly less effective, still retained antibacterial rates above 89% after 15D.

Comparative analysis revealed higher efficacy against *E. coli* (Gram-negative bacteria) than *S. aureus* (Gram-positive bacteria). This difference may arise from structural variations in bacterial cell walls: the outer membrane of Gram-negative bacteria is more permeable to Ag+ ions, while the thick peptidoglycan layer of Gram-positive bacteria partially hinders ion penetration.

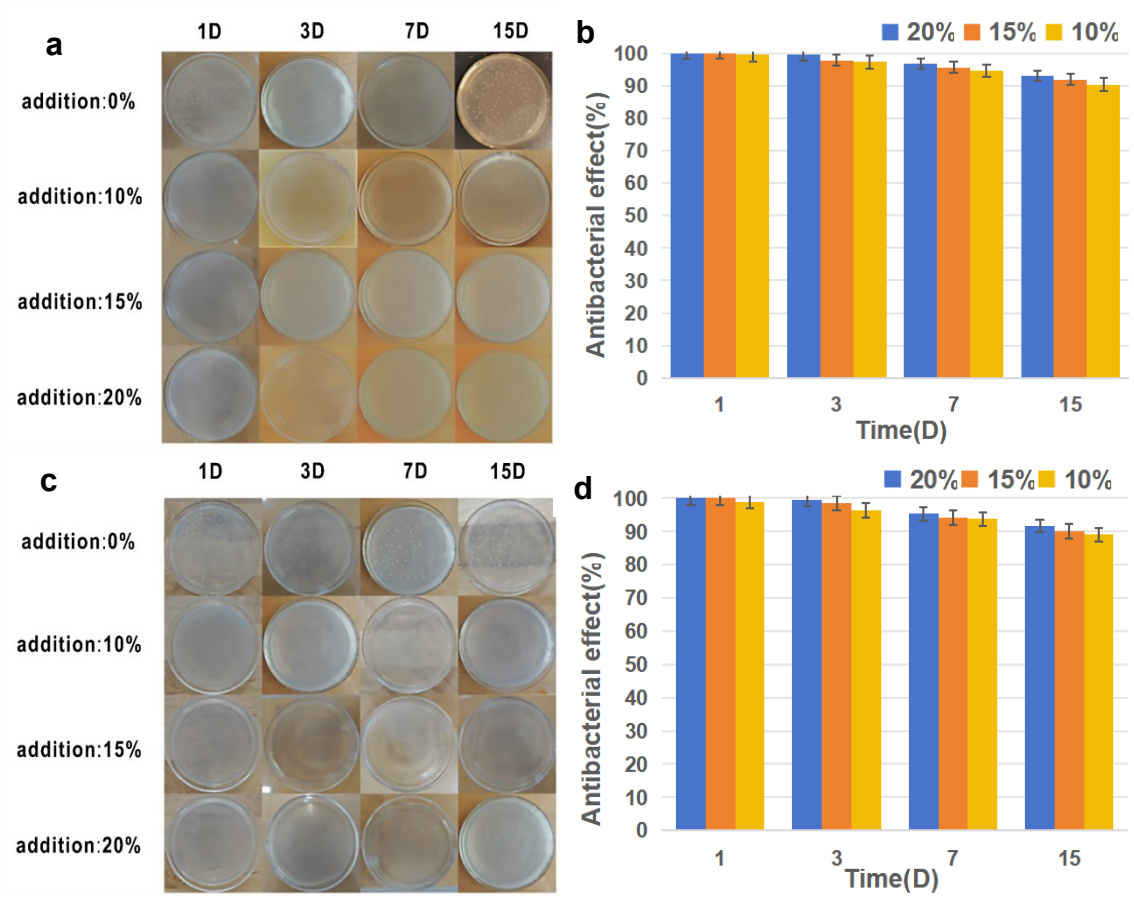

Fig. 6. Antibacterial effect of Ag-TiO_2/EVA antibacterial film on *E. coli* and *S. aureus*: (a) Growth pattern of *E. coli*; (b) the antibacterial rate of Ag-TiO_2/EVA against *E. coli*; (c) Growth status of *S. aureus*; (d) Ag-TiO_2/EVA antibacterial rate against *S. aureus*

Antifungal and Anti-discoloration Performance of Ag-TiO_2/EVA Films on Wood

Efficacy of Ag-TiO_2/EVA films against Botryodiplodia theobromae

As summarized in Table 2, EVA emulsion alone (0% Ag-TiO_2) exhibited limited antifungal activity against *Botryodiplodia theobromae*, with infection scores decreasing marginally from 3.7 to 2.3 as film thickness increased. However, the incorporation of Ag-TiO_2 significantly enhanced control efficacy. At a fixed thickness, higher Ag-TiO_2 loadings drastically reduced infection scores.

When the film thickness ranged between 0.12 and 0.15 mm and the Ag-TiO_2 content was 0%, the infection value was high (3.7) with a very low control efficacy of only 9%. Upon adding 10% Ag-TiO_2, the infection value decreased to 1.7, and the control efficacy significantly improved to 59%, indicating that pure EVA films provided minimal protection against fungal invasion. By contrast, Ag-TiO_2 incorporation enhanced antifungal performance. However, at this low film thickness and 10% Ag-TiO_2 loading, complete protection was unachievable. When the Ag-TiO_2 content was increased to 20%, the infection value dropped to 0 with 100% control efficacy, demonstrating full prevention of *Botryodiplodia theobromae* colonization. Increasing the film thickness also elevates control efficacy: for pure EVA films (0% Ag-TiO_2), thickening the film from 0.12–0.15 mm to 0.21-0.24 mm reduced the infection value from 3.7 to 2.3 and improved control efficacy from 9% to 42%. This suggests that thicker EVA films physically blocked hyphal

penetration due to their superior film-forming properties. At a lower thickness (0.12 to 0.15 mm) with 15% Ag-TiO_2, the infection value was 0.5 (87% control efficacy), confirming that even moderate Ag-TiO_2 loading effectively mitigated fungal invasion under thin-film conditions. Complete suppression of fungal growth (100% efficacy) was achieved under two conditions: (1) films with 0.12 to 0.15 mm thickness and ≥20% Ag-TiO_2, or (2) films with 0.18 to 0.21 mm thickness and ≥15% Ag-TiO_2. The results demonstrate that the Ag-TiO_2/EVA emulsion-derived film exhibited significant control efficacy against *Botryodiplodia theobromae*, effectively protecting wood from fungal infestation.

Table 2. Effect of Ag-TiO_2 Loading and Film Thickness on the Control Efficacy against *Botryodiplodia theobromae*

Film Thickness (mm)	Mass Fraction of A-TiO_2 (%)	Infection Value	Prevention and Control Efficacy
0.12 to 0.15	0	3.7	9
	10	1.7	59
	15	0.5	87
	20	0	100
0.15 to 0.18	0	3.3	21
	10	1.3	67
	15	0.3	94
	20	0	100
0.18 to 0.21	0	2.8	30
	10	0.7	84
	15	0	100
	20	0	100
0.21 to 0.24	0	2.3	42
	10	0.5	89
	15	0	100
	20	0	100

Botryodiplodia theobromae has a prolonged sporulation cycle, typically requiring approximately two months of cultivation, yet its hyphal growth is exceptionally rapid, with a daily growth rate of up to 4.0 cm. Consequently, the fungal infestation of wood primarily occurs through hyphal proliferation across the wood surface and penetration into its internal pore structures. Microstructural observations (Fig. 7) corroborated these results. Untreated wood samples (Fig. 7a) showed extensive fungal colonization, with thick, dense hyphae (yellow arrows) filling the cell lumens. While pure EVA films (Fig. 7b) slightly reduced hyphal density compared to untreated wood, fungal penetration remained widespread, confirming their weak protective effect. In contrast, Ag-TiO_2/EVA films with 15% loadings (Fig. 7c) displayed sparse and underdeveloped hyphae within cells, indicating strong inhibitory activity.

Remarkably, at 20% Ag-TiO_2 (Fig. 7d), no hyphal growth was observed, demonstrating complete prevention of fungal invasion. These findings highlight the critical role of Ag-TiO_2 in enhancing the antifungal performance of EVA films. The nanoparticles likely disrupt fungal cell walls and metabolic processes through sustained release of antimicrobial ions, synergizing with the physical barrier provided by the EVA matrix to achieve superior protection.

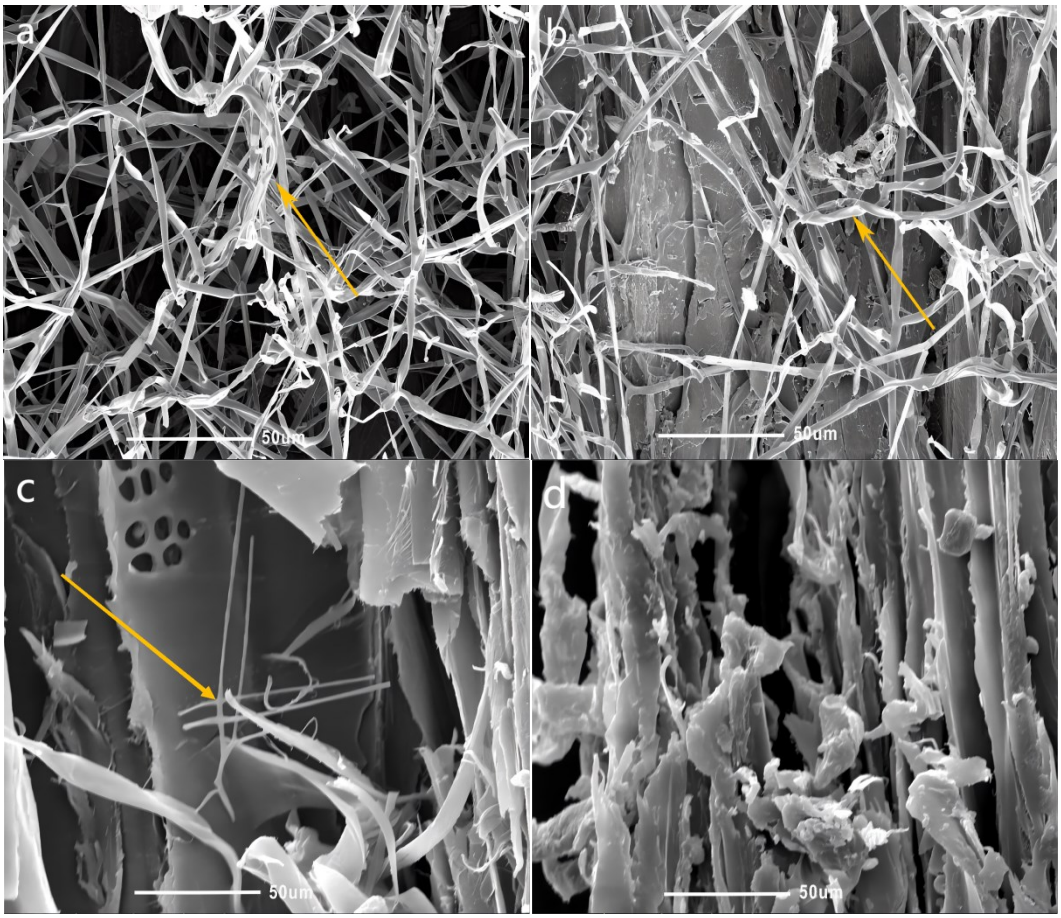

Fig. 7. SEM image of wood sample after *Botryodiplodia theobromae* attack: (a) Materials; (b) 0% control material for addition; (c) 15% additive-treated material; (d) 20%additive-treated material

Efficacy of Ag-TiO_2/EVA films against Aspergillus niger

As shown in Table 3, pure EVA films (0% Ag-TiO_2) exhibited moderate antifungal activity against *Aspergillus niger*, with infection scores decreasing from 3.3 to 2.2 as film thickness increased. However, the addition of Ag-TiO_2 significantly enhanced control efficacy. At a fixed thickness, higher Ag-TiO_2 loadings markedly reduced infection scores. When the film thickness ranged between 0.12 and 0.15 mm and the Ag-TiO_2 content was 0%, the infection value was high (3.3) with a low control efficacy of only 19%. However, compared to *Botryodiplodia theobromae*, the infection value decreased by 0.4 and the control efficacy increased by 10%, indicating that the EVA film exhibited slightly better antifungal performance against *Aspergillus niger* than against *Botryodiplodia theobromae*, though the effect remained insufficient to fully prevent wood infestation. Upon adding 10% Ag-TiO_2, the infection value dropped to 1.5, and the control efficacy significantly improved to 64%, demonstrating enhanced protection against *Aspergillus* niger. However, at this low film thickness and 10% Ag-TiO_2 loading, complete protection was unattainable. Notably, the 5% improvement in control efficacy for *A. niger* under these conditions (compared to *Botryodiplodia theobromae*) suggests comparable antifungal efficacy of Ag-TiO_2 against both fungi. When the Ag-TiO_2 content was increased to 20%, the infection value reached 0 with 100% control efficacy, confirming complete prevention of *Aspergillus niger* colonization.

Table 3. Effect of Ag-TiO_2 Loading and Film Thickness on the Control Efficacy against *Aspergillus niger*

Film Thickness (mm)	Mass Fraction of A-TiO_2 (%)	Infection Value	Prevention and Control Efficacy
0.12 to 0.15	0	3.3	19
	10	1.5	64
	15	0.3	94
	20	0	100
0.15 to 0.18	0	3.2	22
	10	1.2	73
	15	0.2	97
	20	0	100
0.18 to 0.21	0	2.5	39
	10	0.5	88
	15	0	100
	20	0	100
0.21 to 0.24	0	2.2	45
	10	0.3	94
	15	0	100
	20	0	100

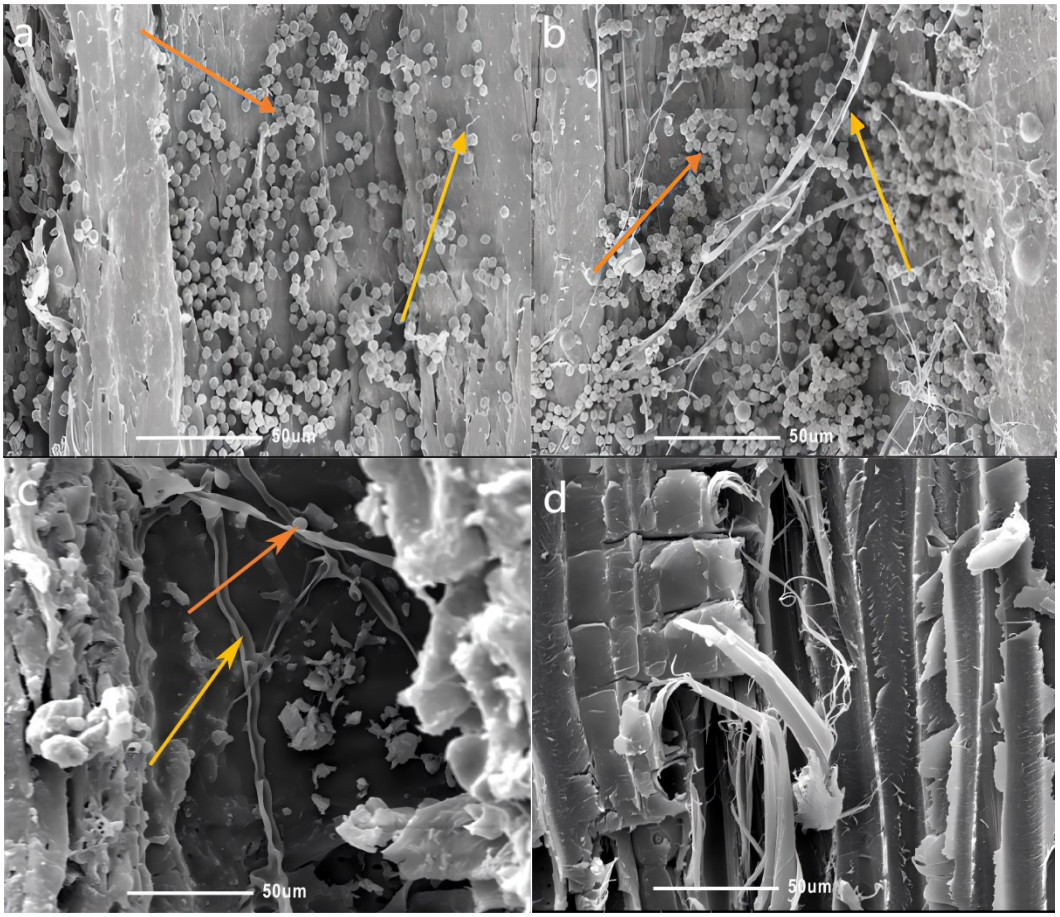

Fig. 8. SEM image of wood sample after *Aspergillus niger* attack: (a) Materials; (b) 0% control material for addition; (c) 15% additive-treated material; (d) 20%additive-treated material

Increasing the film thickness also elevates control efficacy: for pure EVA films (0% Ag-TiO_2), thickening the film from 0.12-0.15 mm to 0.21-0.24 mm reduced the infection value from 3.3 to 2.2 and it improved control efficacy from 19% to 45%. While thicker EVA films partially inhibited *Aspergillus niger* growth through physical barrier effects, the absence of active antimicrobial agents ultimately failed to prevent fungal penetration. At a lower thickness (0.12 to 0.15 mm) with 15% Ag-TiO_2, the infection value was 0.3 (97% control efficacy), demonstrating near-complete suppression of *Aspergillus* niger infestation even under thin-film conditions. Complete suppression of fungal growth (100% efficacy) was achieved under two critical conditions: (1) films with 0.12 to 0.15 mm thickness and ≥20% Ag-TiO_2, or (2) films with 0.18 to 0.21 mm thickness and ≥15% Ag-TiO_2.

Microscopic analysis (Fig. 8) further validated these results. Untreated wood samples (Fig. 8a) displayed extensive colonization by *Aspergillus niger*, with robust hyphae (yellow arrows) and abundant spores (orange arrows) densely distributed within cell lumens and walls. Pure EVA films (Fig. 8b) slightly reduced hyphal and spore density compared to untreated samples, but fungal structures remained intact, confirming limited protection. In contrast, Ag-TiO_2/EVA films with 15% loadings (Fig. 8c) showed sparse, flattened hyphae and significantly fewer spores, indicating suppression of spore germination and disruption of hyphal integrity. Remarkably, at 20% Ag-TiO_2 (Fig. 8d), no hyphae or spores were observed, demonstrating complete inhibition of fungal proliferation.

CONCLUSIONS

1. Using Ag-TiO_2 and ethylene-vinyl acetate (EVA) emulsion as components, the Ag-TiO_2/EVA composite material was synthesized. The particles of this composite material presented a distinct spherical shape. The surface of the small spheres was relatively smooth, and there were point-like substances on it. Some of the spherical surfaces had wrinkled phenomena, and their average particle size was greater than 1 μm.
2. Increasing Ag-TiO_2 loadings significantly enhanced the sustained antibacterial activity against both *Staphylococcus aureus* (Gram-positive) and *Escherichia coli* (Gram-negative). All samples demonstrated >99% bactericidal efficiency within 24 h. After 15 days, the 20% Ag-TiO_2 sample retained 93.01% (*E. coli*) and 91.67% (*S. aureus*) antibacterial efficacies, while the 10% Ag-TiO_2 sample maintained values greater than 89%, underscoring the durability of antimicrobial effects.
3. With increasing Ag-TiO_2 content, the tensile strength of the emulsion-formed film gradually increased, the water vapor transmission rate (WVTR) progressively decreased, while the film adhesion grade remained unchanged at Grade 1. Compared to the 0% Ag-TiO_2 control, tensile strength increased by 19.8%, 24.6%, and 29.3% for incremental loading. Concurrently, at a film thickness of 0.21 to 0.24 mm, water vapor transmission rates decreased by 48.6%, 52.9%, and 60.6%, respectively, demonstrating synergistic enhancement of mechanical integrity and moisture resistance.
4. The antifungal efficacy of the Ag-TiO_2/EVA composite against *Aspergillus niger* and *Botryodiplodia theobromae* was improved with increasing Ag-TiO_2 content. 100% efficacy was achieved under the following conditions: thinner films (0.12 to 0.15 mm thickness) with ≥20% Ag-TiO_2 loading, or thicker films (0.18 to 0.21 mm thickness) with ≥15% Ag-TiO_2 loading.

ACKNOWLEDGMENTS

The authors are grateful for the support of the Jilin Provincial Science and Technology Development Program, Grant No. 20220202090NC、the Innovation Capacity Construction Program of Jilin Provincial Development and Reform Commission, Grant No. 2020C027-2 and Jilin Province Science and Technology Development Project, Grant No. 20250201077GX. The authors also acknowledge the technical support from the Microbial Processing Platform provided by the Jilin Provincial Engineering Research Center of Forestry Biotechnology and the Forestry Biotechnology Innovation Research Platform, College of Forestry, Beihua University.

REFERENCES CITED

Borreguero, A. M., Valverde, J. L., Rodríguez, J. F., Barber, A. H., Cubillo, J. J., and Carmona, M. (2011). "Synthesis and characterization of microcapsules containing Rubitherm® RT27 obtained by spray drying," *Chemical Engineering Journal,* 166(1), 384-390. DOI: 10.1016/j.cej.2010.10.055

Cao, J. (2006). "Current status of wood preservation technologies and research abroad," *Scientia Silvae Sinicae* 1(07), 120-126.

Chen, C., Cheng, X., Wang, L., and Xu, M. (2022). "Study on the decay resistance of modified nano-composite wood preservatives," *Forest Engineering* 38(06), 61-68.

Cui, Y., Zhao, Y., Tian, Y., Zhang, W., Lü, X., and Jiang, X. (2012). "The molecular mechanism of action of bactericidal gold nanoparticles on *Escherichia coli*," *Biomaterials* 33(7), 2327-2333. DOI: 10.1016/j.biomaterials.2011.11.057

Emmerich, L., Bleckmann, M., Strohbusch, S., Brischke, C., Bollmus, S., and Militz, H. (2021). "Growth behavior of wood-destroying fungi in chemically modified wood: Wood degradation and translocation of nitrogen compounds," *Holzforschung* 75(9), 786-797. DOI: 10.1515/hf-2020-0252

GB/T 1037(2021). "Determination of water vapor transmission properties of plastic films and sheets—Cup method (gravimetric)," Standardization Administration of China, Beijing, China.

GB/T 1040.3(2006). "Determination of tensile properties of plastics," National Technical Committee on Plastics of Standardization Administration of China, Beijing, China.

GB/T 18261(2013). "Test method for efficacy of mold preventives against wood molds and stain fungi," Standardization Administration of China, Beijing, China.

GB/T 21866(2008). "Antibacterial coatings—Test method for antibacterial activity and efficacy," Standardization Administration of China, Beijing, China.

GB/T 9286(1998)."Methods for determining the adhesion of paint films," Standardization Administration of China, Beijing, China.

Gunputh, U. F., Le, H., Lawton, K., Besinis, A., Tredwin, C., and Handy, R. D. (2020). "Antibacterial properties of silver nanoparticles grown *in situ* and anchored to titanium dioxide nanotubes on titanium implant against *Staphylococcus aureus*," *Nanotoxicology* 14(1), 97-110. DOI: 10.1080/17435390.2019.1665727

He, X. Y., Kong, F. X., Wang, Y. W., Shao, H. L., Bao, Y. J., Xu, L., and He, X. H. (2021). "Study on wood properties and flooring application of domestic plantation teak," *Forest Engineering* 37 (04), 47-57. DOI: 10.16270/j.cnki.slgc.2021.04.010.

Jian, N. H., Zhao, H. L., and Liu, M. (2022). "Drivers and potential of forest resource

growth in China: Based on the Ninth National Forest Inventory," *Journal of Forestry and Grassland Policy Research* 2(03), 64-71.DOI: 10.12344/lczcyj.2022.09.22.0001

Jin, G., Qin, H., Cao, H., Qian, S., Zhao, Y., Peng, X., and Chu, P. K. (2014). "Synergistic effects of dual Zn/Ag ion implantation in osteogenic activity and antibacterial ability of titanium," *Biomaterials* 35(27), 7699-7713. DOI: 10.1016/j.biomaterials.2014.05. 074

Li, Y., Yang, Y., Qing, Y., Li, R., Tang, X., Guo, D., and Qin, Y. (2020). "Enhancing ZnO-NP antibacterial and osteogenesis properties in orthopedic applications: A review," *International Journal of Nanomedicine* 15, 6247-6262. DOI: 10.2147/IJN. S262876

Lipovsky, A., Gedanken, A., and Lubart, R. (2013). "Visible light-induced antibacterial activity of metaloxide nanoparticles," *Photomedicine and Laser Surgery* 31(11), 526-530. DOI: 10.1089/pho.2012.3339

Mohandas, A., Krishnan, A. G., Biswas, R., Menon, D., and Nair, M. B. (2017). "Antibacterial and cytocompatible nanotextured Ti surface incorporating silver via single step hydrothermal processing," *Materials Science and Engineering: C* 75, 115-124. DOI: 10.1016/j.msec.2017.02.037

Persaud, I., Raghavendra, A. J., Paruthi, A., Alsaleh, N. B., Minarchick, V. C., Roede, J. R., and Brown, J. M. (2020). "Defect-induced electronic states amplify the cellular toxicity of ZnO nanoparticles," *Nanotoxicology* 14(2), 145-161. DOI: 10.1080/ 17435390.2019.1668067

Selim, M. S., Shenashen, M. A., Elmarakbi, A., Fatthallah, N. A., Hasegawa, S. I., El-Safty, and S. A. (2017). "Synthesis of ultrahydrophobic and thermally stable inorganic–organic nanocomposites for self-cleaning foul release coatings," *Chemical Engineering Journal* 320, 653-666. DOI: 10.1016/j.cej.2017.03.067

Sreeja, S., and Shetty, V. (2017). "Photocatalytic water disinfection under solar irradiation by Ag@ TiO_2 core-shell structured nanoparticles," *Solar Energy* 157, 236-243. DOI: 10.1016/j.solener.2017.07.057

Su, Y., Wu, D., Xia, H., Zhang, C., Shi, J., Wilkinson, K. J., and Xie, B. (2019). "Metallic nanoparticles induced antibiotic resistance genes attenuation of leachate culturable microbiota: The combined roles of growth inhibition, ion dissolution and oxidative stress," *Environment international* 128, 407-416. DOI: 10.1016/j.envint.2019. 05.007

Sun, F. L., Kakwara, P. N., Wu, H. P., Qian, J. J., Yang, X. S., Rao, J., and Guo, M. (2017). "Overview of bamboo and wood preservation technologies," *Journal of Forestry Engineering* 2(05), 1-8. DOI: 10.13360/j.issn.2096-1359.2017. 05.001

Shams, S., Khan, A. U., Yuan, Q., Ahmad, W., Wei, Y., Khan, Z. U. H., ... and Ullah, S. (2019). "Facile and eco-benign synthesis of Au@ Fe_2O_3 nanocomposite: efficient photocatalytic, antibacterial and antioxidant agent," *Journal of Photochemistry and Photobiology B: Biology* 199, article 111632. DOI:10.1016/j.jphotobiol.2019.111632.

Teng, T. J., Arip, M. M., Sudesh, K., Nemoikina, A., Jalaludin, Z., Ng, E. P., Lee, and H. L. (2018). "Conventional technology and nanotechnology in wood preservation: A review," *BioResources* 13(4), 9220-9252. DOl: 10.15376/biores.13.4.Teng

Xi, L. X., and Jiang, M. L. (2013). "Advances in triazole wood preservatives," *China Forest Products Industry* 40(04), 3-8. DOI: 10. 19531/j.issn1001-5299.2013.04.001

Yang, L. Z., Li, Y., Qian, H. F., Zhang, H., Qi, X. G., and Wang, L. (2021). "Research progress on application and antibacterial mechanism of natural plant preservatives," *Food and Fermentation Industries* 47(01), 303-308. DOI: 10.13995/j.cnki.11-

1802/ts.024857.
Yang, X. M. (2011). "Application status and environmental/health assessment of CCA," *Journal of Sichuan Forestry Science and Technology* 32(01), 69-73. DOI: 10.16779/j.cnki.1003-5508.2011.01.011
Zhang, H., and Chen, G. (2009). "Potent antibacterial activities of Ag/TiO_2 nanocomposite powders synthesized by a one-pot sol− gel method," *Environmental Science & Technology* 43(8), 2905-2929. DOI: 10.10.1021/es803450f
Zhang, J. B., Huang, H. B., Zhang, C. W., and Guo, M. H. (2016). "Research status and prospects of biomass wood preservatives," *New Chemical Materials* 44(04), 35-37+40.
Zhao, J. X., Zhang, B. P., Li, Y., Yan, L. P., and Wang, S. J. (2012). "Optical and photocatalytic properties of TiO_2/Ag–SiO_2 nanocomposite thin films," *Journal of Alloys and Compounds* 535, 21-26. DOI: 10.1016/j.jallcom.2012.04.089

Article submitted: March 19, 2025; Peer review completed: May 2, 2025; Revised version received: June 15, 2025; Further revised version received: June 16, 2025; Accepted: July 1, 2025; Published: July 11, 2025.
DOI: 10.15376/biores.20.3.7194-7210